Mouse lipin-1 and lipin-2 cooperate to maintain glycerolipid homeostasis in liver and aging cerebellum

Jennifer R. Dwyer[a], Jimmy Donkor[b,1], Peixiang Zhang[b], Lauren S. Csaki[b], Laurent Vergnes[b], Jessica M. Lee[b], Jay Dewald[c], David N. Brindley[c], Elisa Atti[d], Sotirios Tetradis[d], Yuko Yoshinaga[e], Pieter J. De Jong[e], Loren G. Fong[f], Stephen G. Young[a,b,f], and Karen Reue[a,b,f,2]

[a]Molecular Biology Institute, University of California, Los Angeles, CA 90095; [b]Department of Human Genetics, David Geffen School of Medicine at the University of California, Los Angeles, CA 90095; [c]Department of Cell Signaling, University of Alberta, Edmonton, AB, Canada T6G 2H7; [d]School of Dentistry, University of California, Los Angeles, CA 90095; [e]Children's Hospital Oakland Research Institute, Oakland, CA 94609; and [f]Department of Medicine, David Geffen School of Medicine at the University of California, Los Angeles, CA 90095

Edited by Richard J. Havel, Cardiovascular Research Institute, San Francisco, CA, and approved July 26, 2012 (received for review March 28, 2012)

The three lipin phosphatidate phosphatase (PAP) enzymes catalyze a step in glycerolipid biosynthesis, the conversion of phosphatidate to diacylglycerol. Lipin-1 is critical for lipid synthesis and homeostasis in adipose tissue, liver, muscle, and peripheral nerves. Little is known about the physiological role of lipin-2, the predominant lipin protein present in liver and the deficient gene product in the rare disorder Majeed syndrome. By using lipin-2–deficient mice, we uncovered a functional relationship between lipin-1 and lipin-2 that operates in a tissue-specific and age-dependent manner. In liver, lipin-2 deficiency led to a compensatory increase in hepatic lipin-1 protein and elevated PAP activity, which maintained lipid homeostasis under basal conditions, but led to diet-induced hepatic triglyceride accumulation. As lipin-2–deficient mice aged, they developed ataxia and impaired balance. This was associated with the combination of lipin-2 deficiency and an age-dependent reduction in cerebellar lipin-1 levels, resulting in altered cerebellar phospholipid composition. Similar to patients with Majeed syndrome, lipin-2–deficient mice developed anemia, but did not show evidence of osteomyelitis, suggesting that additional environmental or genetic components contribute to the bone abnormalities observed in patients. Combined lipin-1 and lipin-2 deficiency caused embryonic lethality. Our results reveal functional interactions between members of the lipin family in vivo, and a unique role for lipin-2 in central nervous system biology that may be particularly important with advancing age. Additionally, as has been observed in mice and humans with lipin-1 deficiency, the pathophysiology in lipin-2 deficiency is associated with dysregulation of lipid intermediates.

Lipid homeostasis requires a precise balance among cellular lipid species to coordinate the metabolic and structural needs of the cell. The synthesis of glycerolipids serves to transform reactive lipid intermediates into stable lipid components that play key roles in membrane structure (i.e., phospholipids) and cellular lipid storage (i.e., triacylglycerol) (1, 2). Members of the lipin protein family perform the penultimate step in glycerolipid synthesis, dephosphorylation of phosphatidic acid (PA) to diacylglycerol (DAG) (reviewed in refs. 3–5). Three lipin proteins are found in mammals (lipin-1, lipin-2, and lipin-3), and each exhibits phosphatidate phosphatase (PAP) activity, but the specific physiological function of each family member is not well understood. The elucidation of mechanisms that regulate triglyceride storage in various tissues is of interest because of an association between obesity and metabolic dysregulation including insulin resistance, type 2 diabetes, hyperlipidemia, and atherosclerosis (6).

To date, the majority of in vivo studies on lipin protein physiology have involved lipin-1 function. A naturally occurring mutation in the mouse lipin-1 gene causes generalized lipodystrophy (7, 8), and lipin-1–deficient humans have severe myopathy and rhabdomyolysis in childhood (9, 10). These phenotypes correlate with the requirement for lipin-1 to provide PAP activity in adipose tissue and skeletal muscle (11, 12). Growing evidence suggests that in addition to the synthesis of glycerolipids, an important role of lipin-1 is to prevent the accumulation of lipid intermediates in the cell. Lipin-1–deficient tissues in mouse, and lipin-1–deficient muscle in humans, accumulate PA, the substrate of lipin PAP activity (10, 13, 14). PA accumulation in lipin-1–deficient adipose tissue and Schwann cells leads to inappropriate activation of the MAPK/ERK signaling pathway and inhibition of cellular differentiation, contributing to the lipodystrophy and peripheral neuropathy occurring in these mice (13, 14). Lipin-1 can also function as a transcriptional coactivator (15) or corepressor (16). The physiological roles of these activities include the activation of hepatic fatty acid oxidation gene expression in fasting liver (15), and the repression of inflammatory and adipogenic genes in adipocytes (16).

Relatively little is known about the functions of lipin-2 and lipin-3 in vivo. Homozygous mutations in human *LPIN2* lead to the rare disorder known as Majeed syndrome (17–19). Majeed syndrome has been reported thus far in only three families, all residing in the Middle East (20). The hallmarks of the disease are congenital dyserythropoietic anemia and recurrent episodes of osteomyelitis; transient dermatosis may also be present (19, 21). Thus far, three mutant alleles have been identified: a nonsense mutation, a splice site mutation, and a missense mutation involving a highly conserved serine residue (17, 18, 21). The first two mutations are predicted null alleles in which functional lipin-2 protein is not present. The missense mutant protein is stable and exhibits coactivator function similar to lipin-1 protein but lacks PAP activity, indicating that the loss of lipin-2 PAP activity is a defining feature of the disease (22). No human diseases caused by lipin-3 deficiency have been described.

In the mouse, lipin-2 mRNA is expressed most prominently in liver, with substantial levels in other tissues including brain (22), raising the possibility that lipin-2 deficiency may alter glycerolipid metabolism in these tissues. Consistent with a role for lipin-2 PAP activity in liver, knockdown of lipin-2 in isolated hepatocytes leads to reduced PAP activity and triglyceride synthesis (23). Data from in vivo studies are limited, but indicate that lipin-2 levels are regulated by various metabolic perturbations. Mouse lipin-2 protein levels are increased by fasting, obesity,

Author contributions: J.R.D., S.G.Y., and K.R. designed research; J.R.D., J. Donkor, P.Z., L.S.C., L.V., J.M.L., J. Dewald, E.A., and L.G.F. performed research; Y.Y., P.J.D.J., and L.G.F. contributed new reagents/analytic tools; J.R.D., J. Donkor, P.Z., L.S.C., L.V., J. Dewald, D.N.B., S.T., and K.R. analyzed data; and J.R.D., S.G.Y., and K.R. wrote the paper.

The authors declare no conflict of interest.

This article is a PNAS Direct Submission.

[1]Present address: Department of Emergency Medicine, University of California at San Francisco–Fresno, Fresno, CA 93701.

[2]To whom correspondence should be addressed. E-mail: reuek@ucla.edu.

See Author Summary on page 14742 (volume 109, number 37).

This article contains supporting information online at www.pnas.org/lookup/suppl/doi:10.1073/pnas.1205221109/-/DCSupplemental.

consuming a high-fat diet, and treatment with inducers of endoplasmic reticulum stress (23, 24), suggesting a potential role in metabolism of excess fatty acids released from adipose tissue stores or diet.

To gain better insight into the physiological role of lipin-2, we developed and characterized a mouse model of lipin-2 deficiency. We identified in vivo functional interactions between lipin-1 and lipin-2 that contribute to lipid homeostasis in liver and cerebellum, and uncovered a critical role for lipins in the aging brain. These results illustrate how members of a protein family can cooperate to maintain tissue homeostasis, and reveal that the nature of the cooperation may occur in tissue- and age-specific manners.

Results

Generation of Mice with Lipin-2 Deficiency and in Vivo Reporter for Lipin-2 Expression. Lipin-2–deficient mice were developed by homologous recombination in ES cells. The *Lpin2* gene, which comprises 20 exons and spans 67 kb, was inactivated by insertion of a promoterless β-geo gene-trapping cassette into intron 3 (Fig. 1*A*). Transcription of this allele produces a fusion transcript consisting of exons 1 through 3 of *Lpin2* followed by the β-geo cassette, and a corresponding protein with β-gal activity that is expressed under the control of *Lpin2* gene-regulatory elements. Mice that are heterozygous or homozygous for the mutant allele exhibit the expected reductions in *Lpin2* mRNA levels (Fig. 1*B*), and lipin-2 protein is virtually undetectable in the liver of homozygotes (Fig. 1*C*). β-Gal activity was evident in tissues in which we previously detected prominent lipin-2 mRNA expression (22). Thus, there was robust staining in liver within hepatocytes, and prominent staining in the brain in the cerebellum, cerebrum, and hippocampus (Fig. 1*D*). We did not detect staining in several tissues in which lipin-1 accounts for nearly all PAP activity (e.g., white adipose tissue, brown adipose tissue, skeletal muscle) (11, 12).

Hepatic Compensation of Lipin-2 Deficiency by Increased Lipin-1 Protein Levels. As the most prominent site of lipin-2 expression is liver (22, 23) (Fig. 1*D*), we expected that lipin-2–KO mice would have reduced hepatic PAP activity. Instead, we found that PAP activity in liver of the lipin-2–KO homozygous and heterozygous mice was higher than in WT mice (Fig. 2*A*). By contrast, PAP activity in white adipose tissue and skeletal muscle was normal in lipin-2–deficient mice (Fig. 2*A*), consistent with the previous demonstration that lipin-1 is responsible for PAP activity in these tissues (7, 11, 12). Consistent with the lack of impairment in PAP activity in lipin-2–deficient liver, levels of PA and other phospholipid species were normal (Fig. 2*B*).

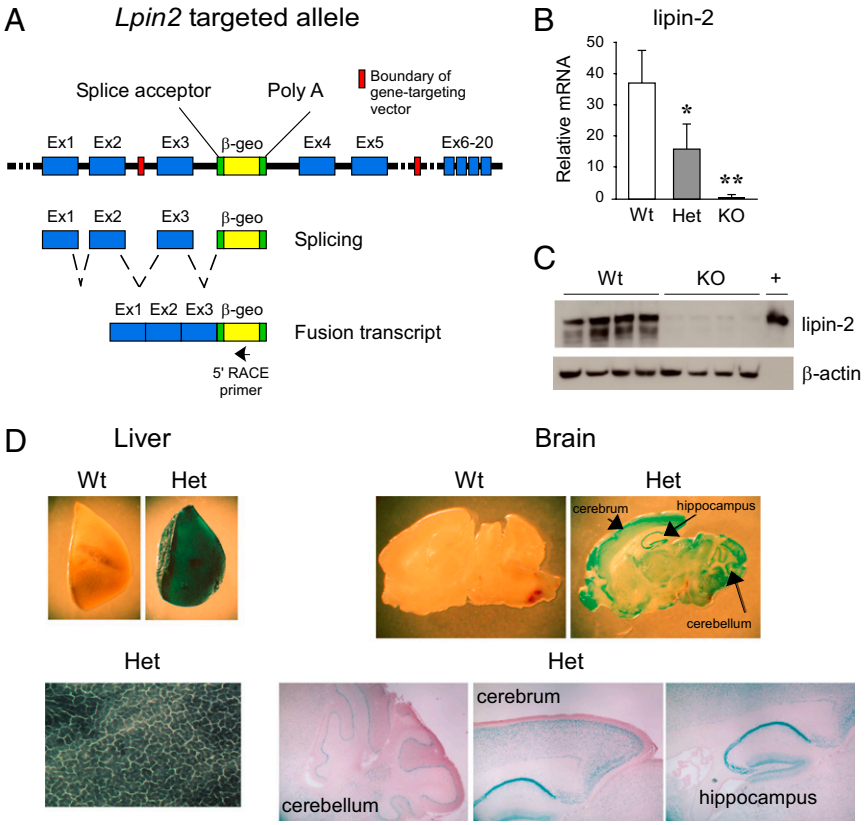

Fig. 1. Inactivation of *Lpin2* by targeted trapping. (*A*) *Lpin2* was inactivated by insertion of the β-geo (fusion of β-gal and neomycin resistance genes) trapping cassette into intron 3 of the gene. Normal gene transcription leads to the production of a fusion mRNA transcript consisting of exons 1 to 3 of *Lpin2* and the β-geo cassette (omits exons 4–20 of *Lpin2*). Targeted cells were identified by 5′ RACE with a β-geo primer (arrow) and by DNA sequencing to confirm expression of a fusion transcript that includes the β-geo gene and extends beyond the 5′ boundary of the targeting vector, into exon 2 of the endogenous *Lpin2* gene. (*B*) Lipin-2 mRNA was quantified in liver of WT ($Lpin2^{+/+}$), heterozygous (Het, $Lpin2^{+/-}$), and KO ($Lpin2^{-/-}$) mice by qPCR ($n = 5$ for each genotype). Values represent mean ± SD (*$P < 0.05$ and **$P < 0.01$ vs. WT). (*C*) Lipin-2 protein was detected in liver of WT or KO mice by using lipin-2–specific antibody. β-Actin was detected as a loading control, and recombinant lipin-2 protein expressed in HEK293 cells was used as a positive control (+). (*D*) Lipin-2–β-geo fusion protein was assessed in tissues of WT and heterozygous mice by staining for β-gal activity. In heterozygous mice, blue staining was most abundant within hepatocytes and the indicated brain regions. Gross sections were magnified 20× to 50×; liver sections were magnified 200×; brain sections were magnified 40×.

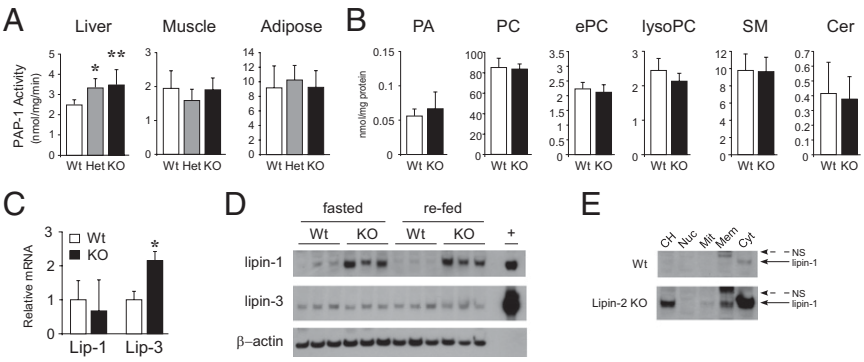

Fig. 2. Enhanced PAP activity and lipin-1 protein expression in lipin-2–KO mice. (*A*) PAP enzyme activity in liver, muscle, and adipose tissue from WT, heterozygous, and KO mice fed a chow diet. Enzyme activity is normalized to cellular protein. (*B*) Total phospholipids were quantified in lipid extracts made from WT and KO liver by ESI-MS and normalized to cellular protein. PC, phosphatidylcholine; ePC, ether-linked PC; SM, sphingomyelin; Cer, ceramides. (*C*) Relative mRNA levels for lipin-1 and lipin-3 were quantified in livers of WT and KO mice by qPCR. In *A*–*C*, $n = 5$ or 6 for each genotype; values represent mean ± SD (*$P < 0.05$ and **$P \leq 0.005$ vs. WT). (*D*) Western blot analysis of lipin-1 and lipin-3 protein levels in liver from fasted and fasted/refed WT and lipin-2–KO mice. β-Actin was used as a loading control, and recombinant lipin proteins were expressed in HEK 293 cells and used as positive controls (+). Note the large increases in lipin-1 protein in lipin-2–deficient samples. (*E*) Subcellular distribution of lipin-1 protein in liver of WT and lipin-2–deficient mice. Hepatic protein lysates were separated into total cell homogenate (CH), nuclear (Nuc), mitochondrial (Mit), membrane (Mem), and cytosolic (Cyt) fractions. Lipin-1 in lipin-2–deficient liver resides primarily in cytosolic and membrane fractions. NS, nonspecific band.

The elevated PAP activity in the liver of lipin-2–deficient mice suggested that that there may be compensatory increases in lipin-1 or lipin-3. Lipin-1 mRNA levels were unchanged, whereas lipin-3 mRNA levels were increased (Fig. 2*C*); however, it should be noted that the absolute levels of lipin-3 mRNA are very low. At the protein level, lipin-1 levels in the liver were far higher in lipin-2–deficient mice than in WT mice in fasted and refed states, whereas similar low levels of hepatic lipin-3 were present in lipin-2 KO and WT liver (Fig. 2*D*). Subcellular fractionation studies showed that the lipin-1 in the liver of lipin-2 KO mice exhibits a similar subcellular distribution to that in WT liver. In both cases, the majority of lipin-1 was present in the cytosol, and a much smaller proportion was associated with the membrane fraction (Fig. 2*E*). The latter includes endoplasmic reticulum (ER) membranes, to which lipin-1 translocates to catalyze the PAP reaction (4). Nuclear lipin-1 levels were very low in WT and lipin-2–KO liver. Thus, the maintenance of PAP activity and phospholipid levels in lipin-2–KO liver are likely a result of compensation by lipin-1 protein.

We assessed whether the increased PAP activity in liver of lipin-2–KO mice correlates with increased hepatic triacylglycerol or circulating lipid levels. On a chow diet, hepatic triacylglycerol and fasting plasma lipid levels (total cholesterol, HDL cholesterol, triglycerides, free fatty acids) in lipin-2–KO mice were similar to those in WT mice (Fig. 3*A* and Table S1). However, when stressed with a high-fat diet (60% fat calories), lipin-2–KO mice accumulated significantly more hepatic triacylglycerol stores than WT mice (Fig. 3*A* and *B*), likely related to higher hepatic PAP activity levels. In contrast, plasma triglyceride and free fatty acid levels were 20% lower in lipin-2–KO mice (Table S1). There were no substantial differences in lipin-2 heterozygous or homozygous null mice in body weight or proportional liver weight on chow or high-fat diets; the gonadal fat pad mass was modestly increased in heterozygous lipin-2–KO compared with WT mice fed a high-fat diet ($P < 0.05$; Fig. S1 *A* and *B*). Thus, the compensation for lipin-2 loss by hepatic lipin-1 largely maintains hepatic and plasma lipid homeostasis in chow fed animals. However, the compensation is imperfect in mice fed a high-fat diet and highlights a requirement for normal levels of lipin-1 and lipin-2 to maintain lipid homeostasis under dietary stress.

In addition to its enzymatic activity, lipin-1 acts as a transcriptional coactivator for expression of fatty acid oxidation genes in the liver (15). To evaluate whether the increased lipin-1 protein present in lipin-2 KO liver had coactivator activity, we quantitated expression levels for known lipin-1 coactivator target genes (15). We found no difference between chow-fed lipin-2–KO and WT mice in hepatic expression of peroxisome proliferator-activated receptor α (*Ppara*), carnitine palmitoyltransferase 1a (*Cpt1a*), and medium chain acyl-CoA dehydrogenase (*Acadm*; Fig. 3*C*). In mice fed a high-fat diet, *Ppara* and *Acadm* expression levels were modestly but significantly reduced in lipin-2–KO liver (Fig. 3*C*). Thus, the elevated levels of lipin-1 protein in lipin-2–KO liver appear not to promote fatty acid oxidation, but likely contribute to enhanced triacylglycerol storage in mice fed a high-fat diet.

Previous work suggests that hepatic lipin-2 has a role in the response to ER stress, particularly in mice fed a high-fat diet (24). We therefore assessed whether the absence of lipin-2 would alter glucose homeostasis or the expression of ER stress markers in mice maintained on chow and high-fat diets. The expression levels for unfolded protein response genes *Chop* (C-EBP homologous protein), *Grp78* (glucose-regulated protein, 78 kDa), and *Xbp1* (X-box binding protein 1, unspliced and spliced forms) were similar in livers of WT and lipin-2–KO mice on chow and high-fat diets, except for a reduction in *Grp78* expression on a chow diet (Fig. 3*D*). Fasting plasma glucose levels were slightly reduced in homozygous KO mice on a chow diet, but this difference was not present in mice fed a high-fat diet, and the KO mice did not appear to have altered glucose tolerance (Fig. S1*C*). These results suggest that a chronic deficiency of lipin-2 does not directly alter hepatic ER stress, potentially because of compensatory changes by other lipin protein family members.

Lipin-2–Deficient Mice Develop Ataxia Associated with Age-Dependent Loss of Lipin-1 in Cerebellum. Throughout development and young adulthood, lipin-2–KO mice were grossly indistinguishable from WT mice. However, beginning at 5 to 6 mo of age, the lipin-2–deficient mice developed a tremor (Fig. 4*A*). The lipin-2–KO mice had an ataxic gait and flicked their tails in a rapid side-to-side movement, most likely to aid in maintaining balance. They were able to rear on their hind legs but typically toppled over after a few seconds. Lipin-2–KO mice exhibited normal grip strength and righting reflex (Fig. S2), but were unable to walk along a balance beam (Fig. 4*B*). WT and heterozygous mice traversed the entire length of wide (2.2 cm) and narrow (1.6 cm) beams nearly 100% of the time without prior training. In contrast, lipin-2–KO mice immediately swung perpendicular to the beam, hung by the

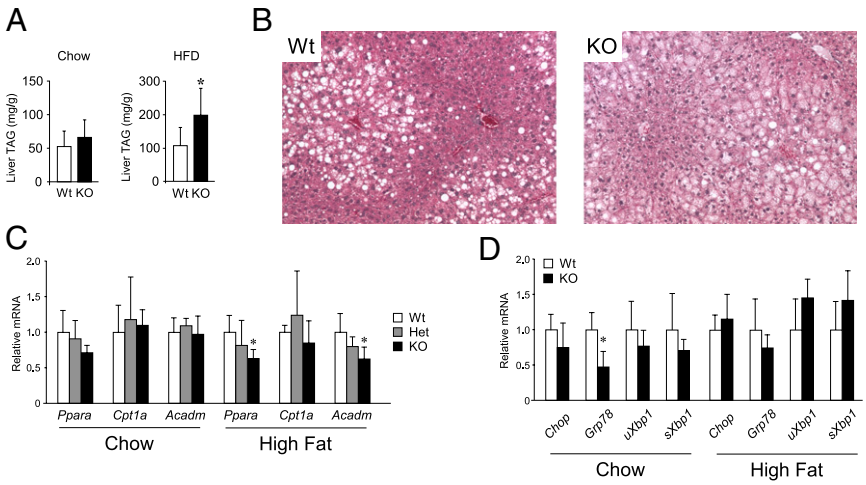

Fig. 3. Lipin-2–KO mice accrue excess hepatic triglyceride on a high-fat diet. (*A*) Hepatic triglyceride (TAG) content in WT and lipin-2–KO mice fed a chow or high-fat diet for 7 wk. Lipid values are normalized to cellular protein (n = 5–6 for each genotype; values represent mean ± SD; *P < 0.05 vs. WT). (*B*) Photomicrographs (magnification of 200×) show representative liver sections from mice fed the high-fat diet and stained with H&E. Lipid accumulation is visible as unstained droplets. (*C*) Expression levels of known lipin-1 coactivator target genes were determined by qPCR in liver samples from WT, heterozygous, and lipin-2–KO mice. *Acadm*, medium chain acyl CoA dehydrogenase; *Cpt1a*, carnitine palmitoyltransferase-1α; *Ppara*, peroxisome proliferator-activated receptor α (n = 5 per genotype; *P < 0.05 vs. WT). (*D*) Expression levels of ER stress genes were determined by qPCR in liver of WT and lipin-2–KO liver. *Chop*, C/EBP homologous protein (also known as DNA-damage-inducible transcript 3); *Grp78*, glucose-regulated protein, 78 kDa (also known as heat shock protein 5); *Xbp1*, X-box binding protein 1, unspliced (uXbp1) and spliced (sXbp1) forms (n = 6–9 per genotype).

forepaws, and fell off within a few seconds (Fig. 4*B*, *Lower*). As the mutant mice did not have impaired grip strength or righting reflex (Fig. S2), the most likely cause for this phenotype was impaired balance.

Lipin-2 is prominently expressed in the cerebellum (Fig. 1*D*), and the ataxic gait in lipin-2–KO mice is reminiscent of human diseases affecting the cerebellum, which is crucial for controlling balance and gait (25, 26). It has been previously demonstrated that PAP activity in the rat cerebellum decreases with age (27–29), but we are aware of no studies that have investigated the role of lipin proteins in cerebellum. Western blot analysis of the three lipin family members was performed in young mice at an age before onset of ataxia in lipin-2–KO mice (2 mo of age), and in old mice at a point when ataxia was severe (10–12 mo of age). In young mice, lipin-1 and lipin-2 proteins were both present in cerebellum, whereas lipin-3 was not detectable (Fig. 4*C*, *Left*). Interestingly, lipin-1 protein levels diminished with age, and nearly undetectable levels of lipin-1 remained in cerebellum of WT and lipin-2–KO mice at 10 to 12 mo of age (Fig. 4*C*, *Right*). Lipin-2 protein levels also decreased in cerebellum of aged WT mice, but remained clearly detectable (Fig. 4*C*). By contrast, lipin-2–KO mice had virtually no remaining lipin proteins at advanced age.

In lipin-1–deficient mice, the accumulation of the PAP enzyme substrate, PA, in Schwann cells and adipose tissue has been implicated in the pathogenesis of peripheral neuropathy and lipodystrophy, respectively (11, 30). This raised the possibility that PA accumulation in lipin-2–KO cerebellum as the mice age contributes to the ataxia. It is also possible that a diminished supply of the PAP product, DAG, could influence intracellular signaling and cerebellar function. We performed electrospray ionization (ESI)-MS on lipid extracts from presymptomatic (2 mo of age) and ataxic (10–12 mo of age) mice. We detected normal PA levels in the young mice (Fig. 4*D*, *Left*), but ataxic lipin-2–KO mice exhibited a 50% increase in total PA levels affecting all of the most abundant PA species (Fig. 4*E*). The PA accumulation was specific for cerebellum and not detected in cerebral cortex (Fig. S3). Several other phospholipid classes, including sphingomyelin and ceramides, were normal in lipin-2–KO cerebellum (Fig. 4 *D* and *E*), aside from modest changes in specific phosphatidylcholine (PC) species (Fig. S4). Total DAG levels were normal in lipin-2–KO mice at both ages assessed, although some individual DAG species exhibited 20% higher or lower levels in aged lipin-2–KO cerebellum (Fig. 4 *D* and *E*). Thus, it appears that lipin-2 activity is not required for the maintenance of DAG levels in the cerebellum, and suggests that insufficient DAG is unlikely to be a major contributor to the phenotype. Together, our results indicate that lipin-2 plays a critical role in maintaining lipid homeostasis in cerebellum as mice age and the levels of lipin-1 protein diminish.

To further define the role of lipin-2 in cerebellum, we localized the protein within this tissue. β-Gal activity staining (Fig. 4*F*) and immunocytochemistry with lipin-2 antibody (Fig. 4*G*) revealed that lipin-2 localizes to the cell layer between the granular and molecular layers of the cerebellum, where Purkinje cells reside. As expected, β-gal staining was not detectable in WT mice, but was robust in the Purkinje cell layer of mice heterozygous for the lipin-2–β-gal allele (Fig. 4*F*, *Center*). Interestingly, the stained cell layer in 10 mo-old lipin-2–KO mice consistently exhibited an irregular appearance, suggesting partial cell loss (Fig. 4*F*, *Right*). Lipin-2 antibody revealed diffuse staining throughout the cytoplasm of cells at the border of the granular and molecular layers, and staining was absent in these cells of lipin-2–KO mice (Fig. 4*G*). Lipin-2 localization to Purkinje cells together with the late-onset ataxia and cerebellar PA accumulation in lipin-2–KO mice suggest a critical function for lipin-2 in maintenance of Purkinje cell lipid homeostasis.

Anemia but No Osteomyelitis in Lipin-2–Deficient Mice. The primary symptoms of Majeed syndrome in humans are dyserythropoietic anemia and recurrent osteomyelitis (20). Reminiscent of humans with Majeed syndrome, the lipin-2–KO mice had mild anemia, with reduced RBC volume and hemoglobin levels, and increased RBC distribution width, indicating the presence of immature erythrocytes (Table 1). However, lipin-2–KO mice studied through 18 mo of age failed to exhibit features of osteomyelitis, such as tail kinks, foot deformities, joint swelling, or thickened ears. We examined tibias from numerous mice of advanced age (n = 13 WT and n = 11 KO mice) for evidence of osteomyelitis by radiography and low-resolution micro-computed tomography (microCT),

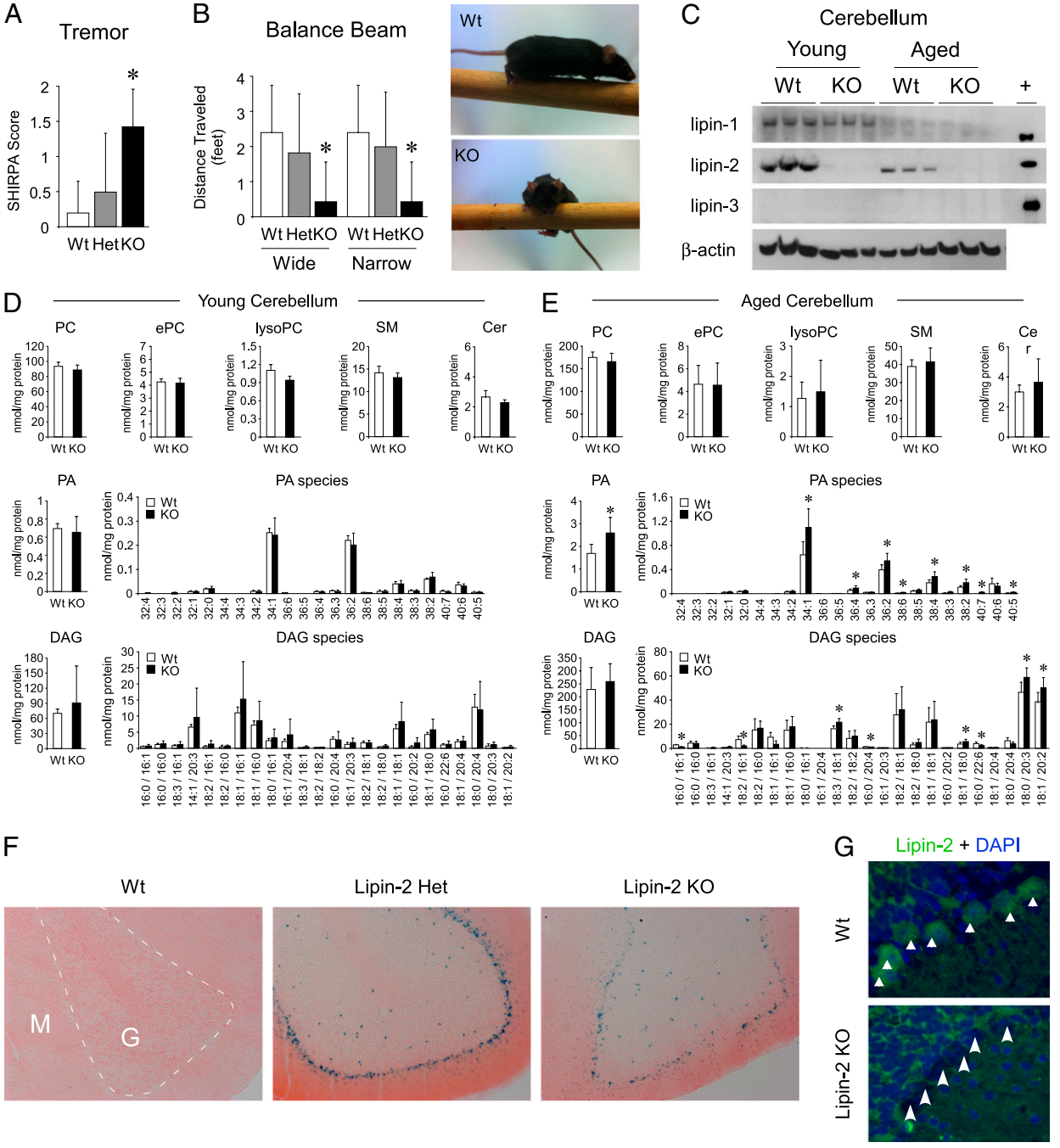

Fig. 4. Lipin-2–KO mice exhibit age-dependent balance impairment associated with phosphatidate accumulation in the cerebellum. (*A*) WT, heterozygous, and lipin-2–KO mice were observed in a viewing jar by an observer blind to genotype, and scored for abnormalities according to SHIRPA guidelines (*Methods*). Lipin-2–deficient mice exhibited a marked tremor that was significantly more apparent compared with WT controls. (*B*) Balance was assessed as the distance traveled on a 3-ft-long beam of wide (2.2 cm) or narrow (1.6 cm) width. WT mice were able to traverse the beam of either width nearly perfectly, but lipin-2–KO mice typically took only a few steps before they turned sideways and dropped from the beam. For *A* and *B*, n = 5 to 7 per genotype. Values represent mean ± SD (*$P < 0.05$ vs. relevant WT). (*C*) Western blot analysis of lipin-1, lipin-2, and lipin-3 protein levels in the cerebellum of young (2 mo) and aged (10–12 mo) mice. In young mice, lipin-1 levels were similar in cerebellum of WT and lipin-2–KO, and lipin-2 levels were robust in WT mice. In older mice, lipin-1 protein was reduced in WT and lipin-2–KO mice, but WT mice maintained detectable lipin-2. Lipin-3 protein was undetectable. β-Actin was used as a loading control and recombinant lipin proteins were expressed in HEK293 and used as positive controls (+). (*D*) Lipid analysis of young (2 mo old) WT and lipin-2–KO cerebellums by ESI-MS. *Top*, Total levels of PC, ether-linked PC (ePC), lysoPC, sphingomyelin (SM), and ceramides (Cer). Lipid values are expressed relative to cellular protein. *Middle*, Total phosphatidate (PA; *Left*) and individual PA species (*Right*) are shown normalized to cellular protein. The molecular species of PA are indicated as total number of carbons:number of double bonds. *Lower*, Total DAG and DAG species (n = 5 per genotype). Values represent mean ± SD (*$P <$ 0.05 vs. WT). (*E*) Lipid analysis of aged (10–12 mo old) WT and lipin-2 KO cerebellums by ESI-MS. Samples are as described in *D* (n = 6–7 per genotype; values represent mean ± SD; *$P < 0.05$ vs. WT). (*F*) Localization of lipin-2 in cerebellar sections of 10-mo-old mice by detection of β-gal activity. Regions of lipin-2–β-gal fusion protein activity are indicated by deep blue color; pink represents eosin counterstain (magnification of 100×). G, granular layer; M, molecular layer. (*G*) Cellular localization of lipin-2 in cerebellum by immunofluorescence using lipin-2 antibody (green). Nuclei are stained with DAPI (blue). Lipin-2 is visible as cytoplasmic staining in large cells located between the molecular and granular layers (arrows, *Top*). The similar regions in lipin-2–KO mice are unstained because of a lack of lipin-2 protein (arrowheads). Diffuse staining of molecular and granular areas is nonspecific (magnification of 882×).

Table 1. Complete blood count analysis

Variable	WT	Het	KO
RBC count, $\times 10^6/\mu L$	10.50 ± 0.58	10.70 ± 0.78	9.82 ± 0.20*
RBC distribution width, %	15.9 ± 0.72	16.8 ± 0.76	17.8 ± 1.18*
Hemoglobin, g/dL	16.4 ± 0.67	16.0 ± 1.27	15.1 ± 0.48*
Platelet count, $\times 10^3/\mu L$	597 ± 16.6	510 ± 83.1	710 ± 82.7*
Platelet volume, fL	4.5 ± 0.08	4.5 ± 0.13	5.0 ± 0.26*

Complete blood cell count was performed on whole blood from WT, heterozygous (Het), and lipin-2 KO mice (n = 5 per genotype). All values represent mean ± SD.
*$P < 0.05$ vs. WT.

but detected no lesions. The lack of osteomyelitis in lipin-2–KO mice suggests that additional genetic or environmental factors in addition to lipin-2 deficiency contribute to osteomyelitis in humans with Majeed syndrome, or that species differences exist.

Deficiency of both Lipin-1 and Lipin-2 Is Lethal. The availability of lipin-1– and lipin-2–deficient mouse models allowed us to ask whether a combined deficiency of both lipin-1 and lipin-2 is tolerated during development. To address this question, *Lpin1*$^{+/-}$*Lpin2*$^{+/-}$ mice were intercrossed and the offspring were screened for viable double-KO mice (*Lpin1*$^{-/-}$*Lpin2*$^{-/-}$). *Lpin1*$^{-/-}$ and *Lpin2*$^{-/-}$ pups were born at the expected Mendelian ratios. We expected to find *Lpin1*$^{-/-}$*Lpin2*$^{-/-}$ pups at a frequency of one in 16, but we never observed any double-KO pups in 282 births, suggesting embryonic lethality (χ^2 test, $P = 0.008$).

To determine when *Lpin1*$^{-/-}$*Lpin2*$^{-/-}$ mice die during embryonic development, we examined embryos at 8.5, 10.5, 11.5, and 12.5 d post coitum (dpc). Double-KO embryos were indistinguishable from other genotypes at 8.5 dpc, but, by 10.5 dpc, they were small, and there was no evidence of a circulatory system (Fig. 5). At 11.5 dpc, all double-KO embryos were dead. Heterozygosity for lipin-1 deficiency with a complete lipin-2–KO background was associated with retarded growth in approximately half the embryos (n = 5 of 11) at 10.5 dpc. Because a deficiency in lipin-1 alone or lipin-2 alone is compatible with normal development, it appears that lipin-1 and lipin-2 can compensate for one another, at least to some degree. However, the embryonic lethality of the double-KO mice shows that lipin-3 cannot compensate for the absence of both lipin-1 and lipin-2.

Discussion

Lipin-1, -2, and -3 PA phosphatase enzymes likely provide the majority of PAP activity for the Kennedy pathway, required for the synthesis of triglycerides as well as PC and phosphatidylethanolamine. To date, in vivo studies have focused on the functions of lipin-1, largely because of the availability of a lipin-1–deficient mouse strain that arose by spontaneous mutation (reviewed in refs. 4, 5, 31). Here, we generated a mouse model to investigate the role of lipin-2 in lipid homeostasis. Characterization of these animals revealed an intricate in vivo relationship between lipin-1 and lipin-2 that acts in a tissue-specific and age-dependent manner (summarized in Fig. 6). In liver, lipin-2 deficiency led to a compensatory increase in hepatic lipin-1 protein and elevated PAP activity, which maintained lipid homeostasis under basal conditions, but led to diet-induced hepatic triglyceride accumulation. As lipin-2–deficient mice aged, they developed ataxia and impaired balance. This was associated with the combination of lipin-2 deficiency and an age-dependent reduction in cerebellar lipin-1 levels, resulting in altered cerebellar phospholipid composition and ataxia. These results highlight a unique role for lipin-2 in cerebellar glycerolipid homeostasis. We also learned that a deficiency of either lipin-1 or lipin-2 is tolerated, but the absence of both enzymes is lethal.

Based on the extremely high levels of lipin-2 protein in liver (22) and the demonstration that knockdown of lipin-2 in isolated hepatocytes reduces PAP activity (23), we expected that lipin-2 KO mice would exhibit a dramatic reduction in hepatic PAP activity and triglyceride content. Surprisingly, PAP activity was instead increased in KO compared with WT liver. This was associated with a compensatory increase in lipin-1 protein levels. This finding highlights a critical difference between the response to acute lowering of lipin-2 expression levels in cultured cells and the chronic loss of endogenous lipin-2 expression in the whole animal. The in vivo response to lack of lipin-2 was an adaptive response that is presumably designed to retain sufficient PAP activity to meet the needs of hepatocytes. Under basal conditions (i.e., chow diet), the compensation by lipin-1 appeared to be adequate to maintain lipid homeostasis in the hepatocytes. However, when subjected to metabolic stress by feeding a high-fat diet, lipin-2–KO mice accumulated excess triglycerides, suggesting that the combined action of lipin-1 and lipin-2 is important for fine-tuned regulation of glycerolipid synthesis under such conditions.

There are many known examples in which genetic deficiency in a given protein is compensated by the activity of a related protein, as occurs in some respects between lipin-1 and lipin-2. However, three aspects of the relationship between lipin-1 and lipin-2 observed here are noteworthy. First, the compensatory increase in lipin-1 levels in lipin-2–deficient mice was tissue-specific, occurring in liver but not in brain. Second, the compensatory increase in lipin-1 occurred through modulation of lipin-1 protein levels without a change in lipin-1 mRNA levels. This suggests a posttranscriptional mechanism that allows rapid changes in protein levels to maintain lipid homeostasis. This is somewhat different from the effects of manipulation of lipin-2 levels in HeLa M cells, which led to changes in lipin-1 mRNA levels (32). Differences may be related to cell/tissue type, the acute or chronic nature of the modulation, and the difference between in vitro and in vivo systems. Third, the increased lipin-1 levels in the liver led to enhanced PAP activity, but did not increase expression levels of genes that are coactivated by lipin-1 via its interaction with PGC-1α (15). This raises the possibility that lipin-2 is required to potentiate the effects of lipin-1 on gene expression. Along these lines, it is interesting that recombinant

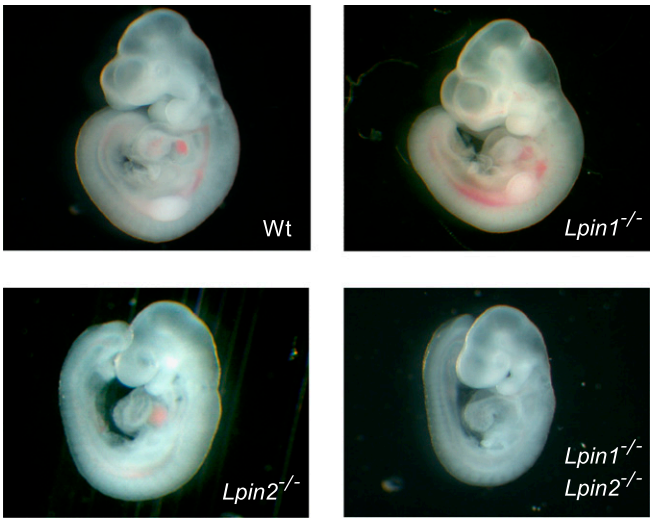

Fig. 5. Combined lipin-1/lipin-2 deficiency is embryonic-lethal. Representative embryos isolated at 10.5 dpc are shown for WT, *Lpin1*$^{-/-}$, *Lpin2*$^{-/-}$, *and Lpin1*$^{-/-}$*Lpin2*$^{-/-}$. *Lpin1*$^{-/-}$*Lpin2*$^{-/-}$ embryos were reduced in size beginning at 9.5 dpc, and could not be recovered much beyond 10.5 dpc.

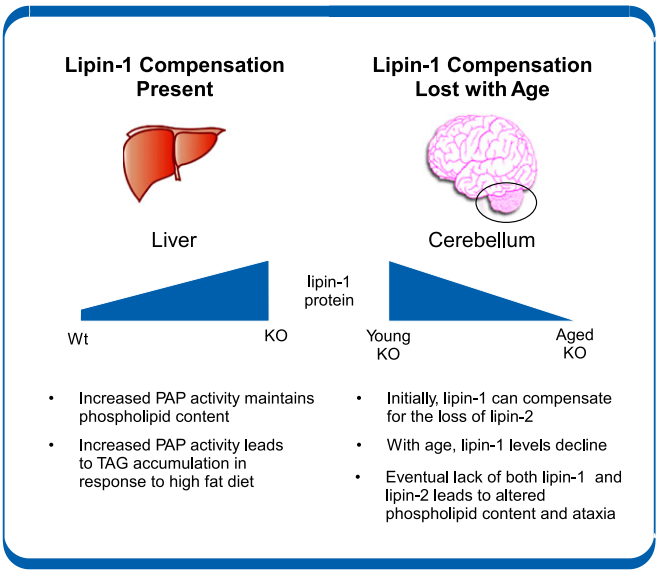

Fig. 6. Tissue pathologic findings seen in lipin-2–deficient mice are governed by the presence or absence of compensation by lipin-1. The effects of lipin-2 deficiency differ among tissues depending on the tissue-specific and age-dependent compensation by lipin-1. In liver of lipin-2–KO mice, lipin-1 protein levels are elevated, leading to maintenance of relatively normal phospholipid levels. However, with a high-fat diet, the increased PAP activity promotes enhanced triacylglycerol storage. In cerebellum of lipin-2 KO mice, lipin-1 levels are similar to those in WT, and decrease with age. This eventual loss of lipin-1 in cerebellum of aged mice on a background of lipin-2 deficiency leads to altered phospholipid content and ataxia.

lipin-1 and lipin-2 proteins appear to form heterodimers (33). The potential functional and physical interaction between lipin-1 and lipin-2, and its role in lipin-1 transcriptional coactivator activity, merits further investigation.

Lipin-2 deficiency resulted in an unexpected central nervous system abnormality: cerebellar disease associated with late-onset ataxia and tremor. This phenotype was 100% penetrant by 6 mo of age, making it possible to identify KO mice simply by observing their gait. Unlike the case with liver, lipin-1 protein levels were not increased to compensate for loss of lipin-2, and analysis of the basis for the late-onset nature of the phenotype revealed an important temporal component to the regulation of lipin proteins in the cerebellum. In young WT mice, lipin-1 and lipin-2 proteins are both expressed in the cerebellum. In young, asymptomatic lipin-2 KO mice, lipin-1 levels in cerebellum are similar to those in WT. Upon aging, the levels of both lipin-1 and lipin-2 diminished in WT cerebellum, but lipin-2 levels remained sufficient to maintain lipid homeostasis and normal cerebellar function. These results are consistent with previous reports of decreasing PAP activity levels within the cerebellum of aging rats (27–29). In contrast to WT mice, aged lipin-2–KO mice experienced an absence of lipin-1 and lipin-2; this was associated with a 50% increase in total PA levels but only minor changes in specific species of other phospholipid classes and DAG. PA has previously been shown to accumulate in tissues of lipin-1–deficient mice and contribute to impaired adipose tissue development and peripheral neuropathy in those animals (13, 14). Recent studies have implicated tissue PA content in several aspects of metabolic homeostasis, including reductions in the expression and activation of peroxisome proliferator-activated receptor-γ (14, 34), activation of ERK signaling (13), inhibition of mammalian target of rapamycin complex 2 (35), inflammatory signaling (36), and others (reviewed in ref. 37). Our studies demonstrate that lipin-2 has a critical role in maintaining PA levels in cerebellum, particularly after loss of lipin-1 during aging.

The lipin-2–KO mice have revealed fundamental information about the role of lipin-2 in glycerolipid homeostasis and its relationship to lipin-1 function in liver and cerebellum. These features of lipin-2 protein function would be very difficult to assess in human patients. Our studies also provided information about the role of lipin-2 deficiency as a determinant of key features of the Majeed syndrome, anemia, and osteomyelitis. As observed in patients with Majeed syndrome, we found that lipin-2 deficiency is sufficient to cause anemia, characterized by reduced blood cell volume and immature erythrocytes (19, 21). However, in contrast to patients with Majeed syndrome, we did not observe swollen joints in our mice, nor did we find osteolytic lesions in bones, as judged by radiography and microCT scans, although we cannot assess whether the mice felt any bone or joint pain. There are various possible explanations for the lack of obvious osteomyelitis in lipin-2–deficient mice. One possibility is that asymptomatic bone lesions might be present but require techniques such as isotope uptake to detect (18, 20). The osteomyelitis in patients with Majeed syndrome is considered to be sterile based on failure to respond to i.v. antibiotic treatment and the inability to culture microorganisms from bone biopsies (21). Nevertheless, the lack of obvious osteomyelitic lesions in lipin-2–KO mice raises the possibility that additional genetic or environmental factors not encountered in our mouse colony (e.g., a fastidious microorganism or virus, or dietary component) act in conjunction with lipin-2 deficiency to promote osteomyelitis in patients with Majeed syndrome. Alternatively, the lack of osteomyelitis in the mice may reflect a species difference in lipin family compensation in bone.

The detection of late-onset ataxia in the lipin-2–deficient mice raises a question about whether patients with Majeed syndrome may be susceptible to similar symptoms. Most patients with Majeed syndrome reported thus far have been studied during the neonatal or early childhood period, with the oldest individual studied at 21 y of age (17, 18, 21). Hence, it is currently unknown to us whether patients with Majeed syndrome may develop neurological syndromes at later stages of life.

In summary, our analysis of lipin-2–deficient mice uncovered unexpected aspects of lipin-2 biology that would not have been predicted based on analysis of lipin-2 tissue expression, by in vitro studies with transfected cells, or by in vivo studies of lipin-2 overexpression with adenoviral vectors (22–24, 32). Our results revealed an intricate in vivo relationship between lipin-1 and lipin-2, with tissue- and age-specific components. In the liver, lipin-2 function can be adequately compensated by an adaptive increase in lipin-1 protein levels under basal conditions, but both proteins are required to maintain lipid homeostasis under the increased lipid load encountered with a high-fat diet. In the central nervous system, lipin-2 has a unique role in maintaining lipid homeostasis in the cerebellum, particularly with advancing age. These studies raise the possibility that lipin-2 levels may be relevant in idiopathic late-onset cerebellar ataxias (38).

Our studies reveal the presence of an intricate relationship between two members of a protein family, and hint that several mechanisms may act in concert to ensure that homeostasis is maintained. Protein families are a common feature of many biological systems, including other enzymes that function in the glycerol-3-phosphate pathway (1, 2). Family members typically have similar molecular activities, raising questions about the physiological significance of the individual members. Future studies will be aimed at further characterizing distinctions and interactions between the members of the lipin protein family that support lipid homeostasis in a tissue-specific and age-dependent manner.

Methods

Mice. *Lpin2*-deficient mice were generated by targeted trapping (39) in ES cells. ES cells were electroporated with the trapping construct consisting of a promoterless β-geo gene (fusion of a β-gal reporter and a neomycin-

resistance gene) with an upstream splice acceptor site (40) inserted into intron 3 of the *Lpin2* gene. ES cells were selected under G418 and targeted cells identified by 5′ RACE with a β-geo primer and DNA sequencing to confirm expression of a fusion transcript that includes the β-geo gene and extends beyond the 5′ boundary of the targeting vector, into exon 2 of *Lpin2*. Targeted ES cells were injected into blastocysts, and resulting chimeras were crossed to C57BL/6J mice to establish germline transmission and backcrossed for four to six generations. WT and mutant alleles were detected by PCR by using primer sets that spanned the β-geo coding sequence within intron 3 or amplified a portion of it, respectively [cctgtctaatgtgcctctcct, agcaggtttagagccatgtga (WT); ttatcgatgagcgtggtggtt, gcgcgtacatcgggcaaataa (mutant)].

Mice were maintained in 12-h light/dark conditions and fed a laboratory chow diet that consisted of 4.5% fat, 50% carbohydrate (wt/wt) (LabDiet; Purina). WT and KO littermates were used for all studies. For specified studies, mice were fed a high-fat diet (35% fat, 33% carbohydrate; Diet F3282, BioServe). Animal studies were approved by the UCLA Animal Research Committee and performed according to guidelines established in the Guide for Care and Use of Laboratory Animals.

Gene Expression Analysis. RNA was extracted using TRIzol (Invitrogen) according to the manufacturer's instructions. cDNA was synthesized and analyzed by quantitative PCR (qPCR) as previously described (41). The qPCR primers sequences were from previous publications (22, 24, 42, 43) and were as follows: *Lpin1* (ccttctatgctgcttttgggaacc; gtgatcgaccacttcgcagagc); *Lpin2* (agttgaccccatcaccgtag, cccaaagcatcagacttggt); *Lpin3* (tggaattgggatgacaaggt, cactgcaagtacccctggt); peroxisome proliferator-activated receptor α, *Ppara* (aatgcaattcgctttggaag, ggccttgaccttgttcatgt); medium chain acyl-CoA dehydrogenase, *Acadm* (aggtttcaagatcgcaatgg, ctccttggtgctccactagc); β-2-microglobulin (cagcatggctcgctcggtgac, cgtagcagttcagtatgttcg); TATA box binding protein, *Tbp* (acccttcaccaatgactcctatg, atgatgactgcagcaaatcgc); 18S ribosomal RNA (accgcagctaggaataatgga, gcctcagttccgaaaacca), carnitine palmitoyltransferase-1α, *Cpt1a* (aaacccaccaggctacagtg, tccttgtaatgtgcgagctg); C/EBP homologous protein, *Chop* (cagtcatggcagctgagtcc, taggtgcccccaatttcatc); glucose-regulated protein, 78 kDa, *Grp78* (tgcagcaggacatcaagttc, tttcttctggggcaaatgtc); unspliced X-box binding protein 1, u*Xbp1* (tatccttttgggcattctgg, aaagggaggctggtaaggaa); and spliced XBP-1, s*Xbp1* (ctgagtccgaatcaggtgcag, gggagtggagtaaggctggt).

Western Blot Analysis of Lipin Proteins. Protein lysates were generated by homogenization of tissues in lysis buffer [250 mM sucrose, 20 mM Tris, 1 mM EDTA, 1.4% Triton X-100, 1× Complete Mini EDTA-free protease inhibitor mixture (Roche Diagnostics) and 1× protein phosphatase inhibitor mixtures 1 and 2 (Sigma)]. Protein lysates were electrophoresed on acrylamide gels, transferred to nitrocellulose membrane, blocked, and incubated with primary antibody. Lipin-1 antibody (used at 1:10,000) (44) was a gift of Maroun Bou Kahlil (University of Ottawa, Ottawa, Canada). Lipin-2 antibody (used at 1:1,000) (23) was a gift of Brian Finck (Washington University, St. Louis, MO). β-Actin antibody (used at 1:5,000) was from Sigma (A1978). Lipin-3 antibody (used at 1:10,000) was from Lifespan Biosciences (C37207). Species-appropriate HRP-conjugated secondary antibodies were used to detect the primary antibody binding by enhanced chemiluminescence (GE Healthcare).

Tissue Histology and Detection of Lipin-2/β-Gal Fusion Protein. Tissues were fixed in 4% paraformaldehyde and embedded in paraffin blocks, and sections were stained with H&E to reveal tissue morphology. β-Gal staining of tissues was performed as previously described (45). Briefly, fresh tissue pieces from WT and lipin-2–deficient mice were placed in prewarmed Solution A (5 mM potassium ferrocyanide, 5 mM potassium ferricyanide, 2 mM $MgCl_2$ in PBS solution, pH 7.5) containing 1.33 mg/mL X-gal and incubated at 37 °C to allow accumulation of product. Samples were then fixed in 10% buffered formalin overnight at 4 °C, rinsed with PBS solution, and digitally imaged under an M8 dissecting microscope (Wild Heerbrugg). For β-gal staining of tissue cryosections, fresh tissues were placed in optimal cutting temperature embedding medium (Tissue-Tek; Sakura Finetek) and frozen on dry ice. Following cryosectioning, samples were fixed in 2% formaldehyde with 0.2% glutaraldehyde for 5 min. Sections were then incubated with Solution A containing X-gal, and counterstained with eosin Y. Images were obtained by using an Eclipse E600 microscope (Nikon) and SPOT imaging software (Diagnostic Instruments).

PAP Activity Assay. PAP activity was measured on tissue extracts essentially as described previously (11, 30). Briefly, fresh mouse tissues were directly homogenized in lysis buffer [250 mM sucrose, 2 mM DTT, protein phosphatase inhibitor mixtures 1 and 2 (Sigma), 1× Complete Mini EDTA-free protease inhibitor mixture (Roche Diagnostics), and 0.15% Tween-20]. PAP-1 activity was measured in 100 mM Tris/HCl buffer, pH 7.4, containing 5 mM $MgCl_2$ and 2 mg/mL fatty acid-poor BSA with 0.6 mM tritiated PA (approximately 6×10^4 dpm labeled with [^{3}H]palmitate) mixed with PA derived from egg PC, 0.4 mM PC, 1 mM EDTA, 1 mM EGTA and 200 μM tetrahydrolipstatin to block the degradation of DAG. Tween-20 was adjusted to a final concentration of 0.05%, and the reactions were incubated at 37 °C. Chloroform containing 0.08% olive oil was added to stop the reaction and basic alumina was added to remove any PA or [^{3}H]palmitate formed by phospholipase A activity. The [^{3}H]DAG product was then isolated and quantified by scintillation counting. Lysate protein amounts and incubation times were optimized to ensure <15% of PA was consumed during incubation. Three different protein concentrations were analyzed for each sample to ensure the proportionality of the assay. Parallel analyses were done in the presence of excess NEM (5 mM) to assess the contribution of lipid phosphate phosphatase activity. This latter activity was subtracted from the total activity to yield true PAP activity values. These assay conditions were chosen to maximize the PAP activity relative to that of lipid phosphate phosphatases.

Metabolic Characterization. Mice were fasted for 5 h (0800 h to 1300 h) before blood and tissue collection. Blood glucose levels were determined with a One Touch Ultra Blood Glucose monitor (Lifescan). Plasma lipids, including triglycerides, free fatty acids, total cholesterol, and HDL cholesterol were quantified as previously described (46). Glucose tolerance tests were performed after a 4.5-h fast by injecting mice i.p. with glucose (2 mg/g body weight) and determining blood glucose levels at 0, 15, 60, and 120 min after injection (47).

Blood Analysis. Complete blood counts were performed on fresh blood samples containing EDTA by using a Hemavet 950 Hematology System (Drew Scientific) at the University of California, Los Angeles, Department of Laboratory and Animal Medicine Diagnostic Laboratory. The following major blood cell groups were quantified: total white blood cells, neutrophils, lymphocytes, monocytes, eosinophils, basophils, total RBCs, and platelets. Mean RBC volume, mean RBC distribution width, hemoglobin concentration, mean corpuscular hemoglobin, mean corpuscular hemoglobin concentration, mean platelet volume, and platelet distribution width were also measured.

Bone Imaging and Analysis. Femurs and tibias from WT and lipin-2–KO mice were dissected, cleaned of soft tissue, and stored in 70% ethanol before radiography and microCT scanning. Femurs and tibias were imaged by using a DX50 Core Specimen Core Radiography system (Faxitron Biooptics/Siemens) with an exposure of 16 s and 35 kV. MicroCT scanning was performed on tibias with a Scanco-40 scanner (Scanco) or a Skyscan 1172 scanner (Skyscan) with the X-ray energy equaling 55 KVp and 72 μA or 55 KVp and 167 μA, respectively. A 0.5-mm aluminum filter and a voxel isotropic resolution of 12 μm were used with both scanners. To evaluate the secondary spongiosa trabecular pattern, 200 slices were measured for each sample covering 2.4 mm of the distal metaphysis starting 0.048 mm below the curvature of the growth plate and moving along the shaft. Contours were drawn in the medullar cavity at a fixed distance from the endosteum, avoiding the cortical bone to define tissue volume. Bone volume, bone volume fraction, connectivity density, and structure model index values were calculated according to the method described by Hildebrand and Rüegsegger (48). A hydroxyapatite phantom was used for density calibration and calculation of apparent density.

Behavioral Analyses. The SHIRPA primary screen is a broad panel of simple behavioral tests that screen for neurological deficits (49). We performed a subset of 14 of these tests that focus on characterizing defects in movement, attention, balance and coordination. We observed WT, heterozygous, and lipin-2–deficient mice, and recorded differences in body position, spontaneous activity, tremor presence, transfer arousal, locomotor activity, gait, pelvic elevation, tail elevation, touch escape, startle response, wire maneuver, righting reflex, contact righting reflex, and negative geotaxis. Each test was scored with a system that categorizes normal and deviant responses to each situation.

Forelimb grip strength was assessed by using a spring scale (8262-M; Ohaus) rigged with a trapeze (50). Each mouse was allowed to grasp the trapeze by its forelimbs and was then gently pulled downward by the tail until it let go. The weight pulled as the mouse released was recorded. A total of five trials were conducted, body weight was subtracted from the weights pulled, and the best three trials were used.

Balance was assessed as the ability of a mouse to traverse a marked 4-ft-long, round balance beam at a height of ~60 cm from the floor. Balance beams with wide (2.2 cm or 5/8″) and narrow (1.6 cm or 3/8″) widths were used. Mice were placed at the 1-ft mark and the distance traveled (as much as 3 ft) was recorded; no time limit was imposed. Mice that fell from the beam were caught in the investigator's hands or on padded material placed below the beam. Mice were given four trials on the wide beam, and the best score was used. Mice were then given two trials on the narrow beam, and the greater distance of these two was recorded.

Quantification of Tissue Lipids. For quantification of hepatic triglycerides, lipids were extracted by a modification of the Bligh and Dyer method (51). Triglyceride concentration was determined using a colorimetric biochemical assay (L-type triglyceride M; Wako). For quantification of phospholipid and DAG species, lipids were prepared from indicated tissues and dried under a gentle stream of argon. An automated ESI-MS approach was used, and data acquisition and analysis and acyl group identification were carried out as described previously (52, 53) with modifications. The lipid samples were dissolved in 1 mL chloroform. An aliquot of 15 to 50 μL of extract in chloroform was used. Precise amounts of internal standards were added, and unfractionated lipid extracts were introduced by continuous infusion into the ESI source on a triple quadrupole mass spectrometer (API 4000; Applied Biosystems). The data were corrected for the fraction of the sample analyzed and normalized to milligrams of cellular protein analyzed.

Immunohistochemistry. Immediately after euthanasia, brains were dissected and placed in 4% paraformaldehyde overnight at 4 °C. The samples were then washed with PBS solution and kept in 70% alcohol until embedding in paraffin. Sections (4 μm) were deparaffinized by using xylenes and graded alcohol washes. Pepsin-mediated antigen retrieval was performed using pepsin (00-3009; Invitrogen) diluted in an equal volume of 0.2 N HCl at 37 °C for 10 min. The sections were blocked with 5% donkey serum in PBS solution for 90 min, and then incubated with Lipin-2 antibody (1:200) (23) at 4 °C overnight in a humidified chamber. Secondary antibody (A21206; 1:1,000; Molecular Probes) was applied to the sections for 1 h in the dark. Nuclear staining was performed with DAPI (0.3 ng/mL) for 30 min, and then the sections were mounted in fluorescent mounting medium (Vectashield). Images were acquired using a Zeiss Observer.D1 microscope outfitted with an AxioCam MRc camera and AxioVision software.

Statistical Analyses. Statistical significance for data involving WT, heterozygous, and KO groups was determined by one-way ANOVA (STATAversion 11) followed by pair-wise comparisons by Student *t* test. Analysis of lipid profile data for PA and PC species was performed by two-way ANOVA followed by pairwise comparisons with Bonferroni correction for multiple comparisons. Analysis of embryonic lethality of $Lpin1^{-/-}Lpin2^{-/-}$ mice was performed by χ^2 test.

ACKNOWLEDGMENTS. We thank Ping Xu and Yan Hu for technical assistance, Dr. Maroun Bou Khalil for lipin-1 antibody, Dr. Brian Finck for lipin-2 antibody, and Bernard Kok for advice on the phosphatidate phosphatase assay. This work was supported by National Institutes of Health (NIH) Grant P01 HL090553 (to L.G.F., S.G.Y, and K.R.), the Canadian Institutes of Health Research (D.N.B.), the Canadian Heart and Stroke Foundation (D.N.B.), and Ruth L. Kirschstein National Research Service Awards GM007185 (predoctoral training support; to J.R.D.) and T32 HG002536 (to J.Donkor and L.S.C.). The lipidomic analyses by MS were performed at the Kansas Lipidomics Research Center Analytical Laboratory, which had instrument acquisition and methods development supported by Kansas Technology Enterprise Corporation; Kansas State University; National Science Foundation Grants EPS 0236913, MCB 0455318, MCB 0920663, and DBI 0521587; and K-IDeA Networks of Biomedical Research Excellence (NIH) Grant P20RR16475.

1. Coleman RA, Lee DP (2004) Enzymes of triacylglycerol synthesis and their regulation. *Prog Lipid Res* 43:134–176.
2. Takeuchi K, Reue K (2009) Biochemistry, physiology, and genetics of GPAT, AGPAT, and lipin enzymes in triglyceride synthesis. *Am J Physiol Endocrinol Metab* 296: E1195–E1209.
3. Carman GM, Han GS (2009) Phosphatidic acid phosphatase, a key enzyme in the regulation of lipid synthesis. *J Biol Chem* 284:2593–2597.
4. Csaki LS, Reue K (2010) Lipins: Multifunctional lipid metabolism proteins. *Annu Rev Nutr* 30:257–272.
5. Harris TE, Finck BN (2011) Dual function lipin proteins and glycerolipid metabolism. *Trends Endocrinol Metab* 22:226–233.
6. Lusis AJ, Attie AD, Reue K (2008) Metabolic syndrome: From epidemiology to systems biology. *Nat Rev Genet* 9:819–830.
7. Péterfy M, Phan J, Xu P, Reue K (2001) Lipodystrophy in the fld mouse results from mutation of a new gene encoding a nuclear protein, lipin. *Nat Genet* 27:121–124.
8. Reue K, Xu P, Wang XP, Slavin BG (2000) Adipose tissue deficiency, glucose intolerance, and increased atherosclerosis result from mutation in the mouse fatty liver dystrophy (fld) gene. *J Lipid Res* 41:1067–1076.
9. Michot C, et al. (2010) LPIN1 gene mutations: A major cause of severe rhabdomyolysis in early childhood. *Hum Mutat* 31:E1564–E1573.
10. Zeharia A, et al. (2008) Mutations in *LPIN1* cause recurrent acute myoglobinuria in childhood. *Am J Hum Genet* 83:489–494.
11. Donkor J, Sariahmetoglu M, Dewald J, Brindley DN, Reue K (2007) Three mammalian lipins act as phosphatidate phosphatases with distinct tissue expression patterns. *J Biol Chem* 282:3450–3457.
12. Harris TE, et al. (2007) Insulin controls subcellular localization and multisite phosphorylation of the phosphatidic acid phosphatase, lipin 1. *J Biol Chem* 282: 277–286.
13. Nadra K, et al. (2008) Phosphatidic acid mediates demyelination in *Lpin1* mutant mice. *Genes Dev* 22:1647–1661.
14. Zhang P, Takeuchi K, Csaki LS, Reue K (2012) Lipin-1 phosphatidic phosphatase activity modulates phosphatidate levels to promote peroxisome proliferator-activated receptor γ (PPARγ) gene expression during adipogenesis. *J Biol Chem* 287: 3485–3494.
15. Finck BN, et al. (2006) Lipin 1 is an inducible amplifier of the hepatic PGC-1alpha/PPARalpha regulatory pathway. *Cell Metab* 4:199–210.
16. Kim HB, et al. (2010) Lipin 1 represses NFATc4 transcriptional activity in adipocytes to inhibit secretion of inflammatory factors. *Mol Cell Biol* 30:3126–3139.
17. Al-Mosawi ZS, Al-Saad KK, Ijadi-Maghsoodi R, El-Shanti HI, Ferguson PJ (2007) A splice site mutation confirms the role of LPIN2 in Majeed syndrome. *Arthritis Rheum* 56: 960–964.
18. Ferguson PJ, et al. (2005) Homozygous mutations in LPIN2 are responsible for the syndrome of chronic recurrent multifocal osteomyelitis and congenital dyserythropoietic anaemia (Majeed syndrome). *J Med Genet* 42:551–557.
19. Majeed HA, Al-Tarawna M, El-Shanti H, Kamel B, Al-Khalaileh F (2001) The syndrome of chronic recurrent multifocal osteomyelitis and congenital dyserythropoietic anaemia. Report of a new family and a review. *Eur J Pediatr* 160:705–710.
20. Majeed HA, El-Shanti H (2008) *GeneReviews*, eds Pagon RA, Bird TD, Dolan CR, Stephens K (Univ Washington, Seattle).
21. Majeed HA, et al. (1989) Congenital dyserythropoietic anemia and chronic recurrent multifocal osteomyelitis in three related children and the association with Sweet syndrome in two siblings. *J Pediatr* 115:730–734.
22. Donkor J, et al. (2009) A conserved serine residue is required for the phosphatidate phosphatase activity but not the transcriptional coactivator functions of lipin-1 and lipin-2. *J Biol Chem* 284:29968–29978.
23. Gropler MC, et al. (2009) Lipin 2 is a liver-enriched phosphatidate phosphohydrolase enzyme that is dynamically regulated by fasting and obesity in mice. *J Biol Chem* 284: 6763–6772.
24. Ryu D, et al. (2011) Endoplasmic reticulum stress promotes LIPIN2-dependent hepatic insulin resistance. *Diabetes* 60:1072–1081.
25. Grüsser-Cornehls U, Bäurle J (2001) Mutant mice as a model for cerebellar ataxia. *Prog Neurobiol* 63:489–540.
26. Morton SM, Bastian AJ (2004) Cerebellar control of balance and locomotion. *Neuroscientist* 10:247–259.
27. Giusto NM, Salvador GA, Castagnet PI, Pasquaré SJ, Ilincheta de Boschero MG (2002) Age-associated changes in central nervous system glycerolipid composition and metabolism. *Neurochem Res* 27:1513–1523.
28. Pasquaré SJ, Ilincheta de Boschero MG, Giusto NM (2001) Aging promotes a different phosphatidic acid utilization in cytosolic and microsomal fractions from brain and liver. *Exp Gerontol* 36:1387–1401.
29. Pasquaré SJ, Salvador GA, Giusto NM (2004) Phospholipase D and phosphatidate phosphohydrolase activities in rat cerebellum during aging. *Lipids* 39:553–560.
30. Kok BP, Kienesberger PC, Dyck JR, Brindley DN (2012) Relationship of glucose and oleate metabolism to cardiac function in lipin-1 deficient (fld) mice. *J Lipid Res* 53: 105–118.
31. Reue K, Brindley DN (2008) Thematic review series: Glycerolipids. Multiple roles for lipins/phosphatidate phosphatase enzymes in lipid metabolism. *J Lipid Res* 49: 2493–2503.
32. Grimsey N, et al. (2008) Temporal and spatial regulation of the phosphatidate phosphatases lipin 1 and 2. *J Biol Chem* 283:29166–29174.
33. Liu GH, et al. (2010) Lipin proteins form homo- and hetero-oligomers. *Biochem J* 432: 65–76.
34. Stapleton CM, et al. (2011) Lysophosphatidic acid activates peroxisome proliferator activated receptor-γ in CHO cells that over-express glycerol 3-phosphate acyltransferase-1. *PLoS ONE* 6:e18932.
35. Zhang C, et al. (2012) Glycerolipid signals alter mTOR complex 2 (mTORC2) to diminish insulin signaling. *Proc Natl Acad Sci USA* 109:1667–1672.
36. Grkovich A, Dennis EA (2009) Phosphatidic acid phosphatase in the regulation of inflammatory signaling. *Adv Enzyme Regul* 49:214–221.
37. Brindley DN, Pilquil C, Sariahmetoglu M, Reue K (2009) Phosphatidate degradation: phosphatidate phosphatases (lipins) and lipid phosphate phosphatases. *Biochim Biophys Acta* 1791:956–961.
38. Brusse E, Maat-Kievit JA, van Swieten JC (2007) Diagnosis and management of early- and late-onset cerebellar ataxia. *Clin Genet* 71:12–24.

39. Friedel RH, Soriano P (2010) Gene trap mutagenesis in the mouse. *Methods Enzymol* 477:243–269.
40. Friedel RH, et al. (2005) Gene targeting using a promoterless gene trap vector ("targeted trapping") is an efficient method to mutate a large fraction of genes. *Proc Natl Acad Sci USA* 102:13188–13193.
41. Phan J, Péterfy M, Reue K (2004) Lipin expression preceding peroxisome proliferator-activated receptor-gamma is critical for adipogenesis in vivo and in vitro. *J Biol Chem* 279:29558–29564.
42. Donkor J, Sparks LM, Xie H, Smith SR, Reue K (2008) Adipose tissue lipin-1 expression is correlated with peroxisome proliferator-activated receptor alpha gene expression and insulin sensitivity in healthy young men. *J Clin Endocrinol Metab* 93:233–239.
43. Zhang P, O'Loughlin L, Brindley DN, Reue K (2008) Regulation of lipin-1 gene expression by glucocorticoids during adipogenesis. *J Lipid Res* 49:1519–1528.
44. Bou Khalil M, et al. (2009) The level and compartmentalization of phosphatidate phosphatase-1 (lipin-1) control the assembly and secretion of hepatic VLDL. *J Lipid Res* 50:47–58.
45. Vergnes L, Chin R, Young SG, Reue K (2011) Heart-type fatty acid-binding protein is essential for efficient brown adipose tissue fatty acid oxidation and cold tolerance. *J Biol Chem* 286:380–390.
46. Barajas B, et al. (2011) NF-E2-related factor 2 promotes atherosclerosis by effects on plasma lipoproteins and cholesterol transport that overshadow antioxidant protection. *Arterioscler Thromb Vasc Biol* 31:58–66.
47. Vergnes L, et al. (2006) Agpat6 deficiency causes subdermal lipodystrophy and resistance to obesity. *J Lipid Res* 47:745–754.
48. Hildebrand T, Rüegsegger P (1997) Quantification of bone microarchitecture with the structure model index. *Comput Methods Biomech Biomed Engin* 1:15–23.
49. Rogers DC, et al. (1997) Behavioral and functional analysis of mouse phenotype: SHIRPA, a proposed protocol for comprehensive phenotype assessment. *Mamm Genome* 8:711–713.
50. Hockly E, et al. (2002) Environmental enrichment slows disease progression in R6/2 Huntington's disease mice. *Ann Neurol* 51:235–242.
51. Bligh EG, Dyer WJ (1959) A rapid method of total lipid extraction and purification. *Can J Biochem Physiol* 37:911–917.
52. Devaiah SP, et al. (2006) Quantitative profiling of polar glycerolipid species from organs of wild-type Arabidopsis and a phospholipase Dalpha1 knockout mutant. *Phytochemistry* 67:1907–1924.
53. Welti R, et al. (2002) Profiling membrane lipids in plant stress responses. Role of phospholipase D alpha in freezing-induced lipid changes in Arabidopsis. *J Biol Chem* 277:31994–32002.